IEEE Access
Multidisciplinary | Rapid Review | Open Access Journal

Received October 27, 2019, accepted November 11, 2019, date of publication November 19, 2019,
date of current version December 6, 2019.

Digital Object Identifier 10.1109/ACCESS.2019.2954408

Trajectory Following and Improved Differential Evolution Solution for Rapid Forming of UAV Formation

LEI BIAN, WEI SUN, AND TIANYE SUN
School of Aerospace Science and Technology, Xidian University, Xi'an 710071, China
Corresponding author: Wei Sun (wsun@xidian.edu.cn)

This work was supported in part by the National Nature Science Foundation of China (NSFC) under Grant 61671356.

ABSTRACT In this paper we proposed the circle trajectory assembly algorithm to control the multi-UAVs circular assembly formation. CTFAP solution provides rapid formation of UAVs on a circular orbit and solve the problem of large scattering distance. Proposed Distributed model prediction control framework improves the optimization ability and reduces the computation consumption with the better convergence ability of the UAV formation. Firstly, a circular trajectory following algorithm with an adaptive parameter is proposed to complete the rapid formation of UAVs on a circular orbit and solve the problem of large scattering distance during formation forming. Then, in the stage of formation reconfiguration, with distributed model prediction control framework (DMPC), the proposed method gets the prediction information of DMPC to optimize the population of classical differential evolution (DE) algorithm and improve the iterative optimization ability of DE algorithm. Experiments show that the proposed differential evolution algorithm greatly improves the efficiency of solving the formation reconfiguration problem under the DMPC framework and overcomes the disadvantages of random population of classical DE. For the proposed rapid forming method, assembly range is reduced by 41% compared with direct linearly formation assembly, and the formation forming time is reduced by approximately 21%. Compared with other optimization algorithms such as Particle Swarm Optimization (PSO), Genetic Algorithm (GA) and DE, the proposed differential evolution algorithm reduces instruction response time of single-drones by 16%-30%.

INDEX TERMS Multi-UAVs, formation molding, DMPC, DE, formation reconfiguration.

I. INTRODUCTION

Multi-UAV formation flying includes both the assembly, maintenance and reconstruction of formation flights, as well as the planning and organization of flying tasks [1]. The distance between adjacent UAVs is required to be safe and the formation stability during flight should be maintained. In the process of mission execution, UAV formation can greatly improve the efficiency of mission execution, such as cooperative reconnaissance, tracking and maintenance, perceptual recognition and cooperative attack; In the actual environment, the frequent changes of tasks and environments require that each drone in the formation must be able to perform flexible position transformation, avoid obstacles [2]–[6] and complete the reconstruction of the formation. UAV formation must be reconstructed to ensure the performance of formation execution; includes formation gathering, target formation reconstruction and formation preservation in formation flying. Many scholars have done a lot of research on UAV formation reconfiguration methods.

At present, the main methods to realize multi-UAV formation forming and reconfiguration include: the artificial potential field method [7], the bionic algorithm and the optimization control method [8]–[10]. In the case of the large-scale formation and the dynamic transformation, artificial potential field method is difficult to make a mathematical model and easy to fall into local optimum. Bionic algorithms include the ant colony algorithm, the fish swarm algorithm, the particle swarm algorithm etc. The computational efficiency of these algorithms is low, but real-time performance in real application determines the stability of

The associate editor coordinating the review of this manuscript and approving it for publication was Luigi Biagiotti.

the formation control. Woods [11] et al. proposed a control method based on potential energy function. However, with the increasing in quantity of drones and the rising of formation size, the drones added later will have an undesirable consequence on the potential energy function of the formation. The more drones in the formation, the explosive growth the potential energy function will be. Ru [12] et al. designed a Distributed Model Predictive Control (DMPC) method based on Nash bargaining to solve the reconfiguration function of the multi-UAV formation. However, it does not take the communication distance constraint of UAVs into the formation mathematical model. Zhang [13] et al. adopted an improved differential evolution algorithm to solve the optimal control variables in the multi-UAV global reconfiguration process, and considered various constraints based on the real-world scenarios. But this algorithm has a large amount of computing burden to solve the control variables. Already have proposed a hybrid particle swarm optimization and genetic algorithm for multi-UAV formation [14], it achieved good optimization results. However, this algorithm has some shortcomings: the large amount of calculation, unfavorable tracking at the node, and difficulty in adapting to changing size of the formation to generate an optimal trajectory.

A new perspective on rapid forming of UAV formation is proposed. We divide the formation forming into two stages: the formation assembly and the target formation reconfiguration. A fast optimization method for asynchronous take-off, circle assembly and rapid reconfiguration of UAV formations is proposed. Firstly, we propose a circle tracking algorithm with self-adaptive parameters, which can quickly complete the flight assembly when multiple UAVs take off asynchronously, we solve the problem that the formation scattering space is too large before the formation assembly. Secondly, the UAV formation reconfiguration method based on Distributed Model Predictive Control (DMPC) was proposed to transform the centralized UAV formation reconfiguration problem into the distributed optimization problem [15] of single UAV flying control. The improved differential evolution algorithm proposed in this paper inherits the prediction information of DMPC, introduces the population optimization operation for classical differential evolution (DE) algorithm. The proposed DE algorithm effectively solves the control quantities in the mathematical model of multi-UAV formation reconfiguration. At the same time, it is faster, more efficient, and meets the real-time requirements of the multi-UAV formation system.

The content of this paper is arranged as follows: Section I is the introduction; Section II discusses the proposed adaptive circular trajectory following algorithm for multi-UAV assembly of asynchronous take-off; Section III introduces the proposed improved DE algorithm based on DMPC framework (Pre-DMPC-DE) in detail; Section IV gives the experiments of the proposed formation forming and reconfiguration algorithms and some comparable results; Finally, the conclusion of this paper is given.

II. ASSEMBLY OF MULTI-UAV IN CIRCULAR TRACK

This paper proposes an assembly method of multi-UAV in the circular track for the formation with asynchronous take-off. First, the multi-UAV formation assembly in the preset circular track after take-off. After the assembly is completed, target formation will be completed by formation reconfiguration. The method can reduce the dispersion interval of the multi-UAV formation, guarantee the communication performance between the UAVs, and provide a good initial formation for the formation reconfiguration.

A. THE MATHEMATICAL MODEL OF UAV

Roger M proposes a new robust controller, which is applied to the regulation and trajectory tracking tasks of four rotor vehicles [26]–[30]. The simulation results show that the scheme is superior and robust to different types of disturbances. It has great inspiration for our algorithm in this paper. we propose an assembly method of multi-UAV in the circular track for the formation with asynchronous departure. First, the multi-UAV formation assembly in the preset circular track after departure. After the assembly is completed, the flying of the target formation will be completed by the formation reconstruction. The method can reduce the dispersion interval of the multi-UAV formation, ensure the communication performance between the formations, and provide a good initial formation for the formation reconstruction.

$$\begin{cases} x(k+1) = x(k) + V(k)\cos\gamma(k)\cos\chi(k)dt \\ y(k+1) = y(k) + V(k)\cos\gamma(k)\sin\chi(k)dt \\ h(k+1) = h(k) - V(k)\sin\gamma(k)dt \\ V(k+1) = V(k) + a(k+1)dt \\ \chi(k+1) = \chi(k) + \chi'(k+1)dt \\ \gamma(k+1) = \gamma(k) + \gamma'(k+1)dt \end{cases} \tag{2-1}$$

In formula (2-1), x, y, h is the projection coordinate of the UAV's centroid position in the ground coordinate system; v, χ, γ are the acceleration, the heading angle and the pitch angle of the UAV; a, χ', γ' are the acceleration, the heading angular velocity and the pitch angular velocity; dt is the sampling period.

The state variables and control variables of either UAV at k moment are $\mathrm{X}_i(k)$ and $U_i(k)$ in formula (2-2):

$$\begin{aligned} \mathrm{X}_i(k) &= [x_i(k), y_i(k), h_i(k), V_i(k), \chi_i(k), \gamma_i(k)] \\ U_i(k) &= [a_i(k), \chi_i(k), \gamma_i(k)] \end{aligned} \tag{2-2}$$

Then the motion formula of the either UAV at k moment is formula (2-3):

$$\mathrm{X}_i(k+1) = f_i\left(X_i(k), \mathrm{U}_i(k)\right) \tag{2-3}$$

B. CIRCLE TRAJECTORY FOLLOWING ALGORITHM WITH THE ADAPTIVE PARAMETER

For a preset circular assembly flying orbit [17], the parameters in the traditional trajectory following algorithm [18] are

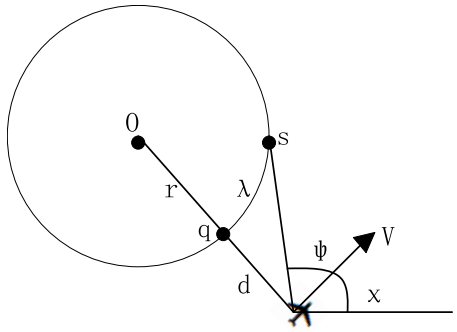

FIGURE 1. Schematic diagram of the CTFAP algorithm.

experimental or empirical values. The Non-adaptive parameter causes the oscillation problem of following the trajectory, as shown in Figure 2(a). The blue circle is the set assembly trajectory, the lower right triangle is the take-off point of UAVs [31]–[33]. After takeoff, the UAV needs to fly along the set circular trajectory. All the UAVs complete the trajectory following and then reconstruct the target formation ('gable' or 'diamond'). In Figure 2, Two UAVs (UAV1 UAV2)with the speeds of $100m/s$ and $200m/s$ track the circular trajectory. The trajectory following algorithm with a fixed parameter of $\lambda = 0.1$ has a large oscillating situation in the 2th UAV. UAV2 can converge to the circular trajectory after nearly a circle of flight, at this time, the parameters show good convergence performance for UAV1. For fast trajectory flowing for takeoff UAVs with individual difference we propose a solution for the circle trajectory following algorithm with the adaptive parameter (CTFAP) to complete the assembly flying of the UAV on the orbit, avoiding the oscillation shown in Figure 2(a).

CTFAP algorithm is shown as following:

Step 1: As shown in Figure 1, a UAV with the heading angle of χ is located outside the circular path. By the parameters of the preset circle trajectory and the position of the UAV, the projection point of the UAV on the circular trajectory can be obtained.

Step 2: The parameter λ is initially set to the median of the best interval. Combining the projection point q with the parameter λ, the sampling point s of the UAV on the circular trajectory can be figured out which is the offset point from point q by the angle λ. (The best interval is $[2\arcsin(V * dt/2R), 2\arcsin(\sqrt{1-(1-a\%)^2}]$, which is solved in Section II.C.)

Step 3: Get the angle ψ between the speed direction of the UAV and the direction of the UAV to the offset sampling point s. The angle λ is brought in the formula (2-4) to get the control amount $u_i(k+1)$ of the UAV in the next moment:

$$\chi'(k+1) = \begin{cases} \psi, if : \|\psi\| \le \chi'_{\max} * dt \\ \chi'_{\max} * dt \end{cases}$$
$$u_i(k+1) = [0, \chi'(k+1), 0] \quad (2\text{-}4)$$

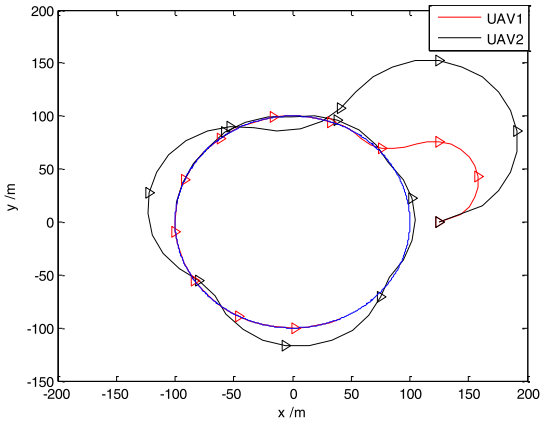

(a) The tracks of the traditional trajectory following algorithm

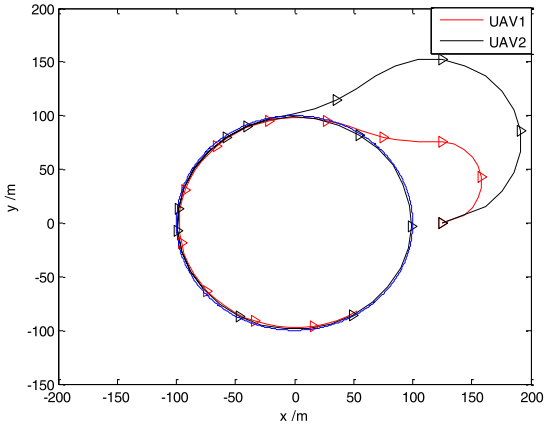

(b) The tracks of CTFAP algorithm

FIGURE 2. Comparison of the traditional trajectory following algorithm and the algorithm with adaptive parameter.

Step 4: Apply the control variable to the control of the UAV in the next moment.

Figure 2(b) shows the experimental results of the improved circle trajectory following assembly algorithm with the adaptive parameter [3], [34], [35]. The blue circle is the set assembly trajectory, the lower right triangle is the take-off point of UAVs. It shows that both UAV1 and UAV2 have good convergence performance. The experimental results show that the automatic parameter interval of the algorithm is correct, which can make the multi-UAV formation quickly to enter the stable circular trajectory assembly state. Compared with the method with the empirical parameter, this algorithm can dynamically adjust in real time under any circumstances to ensure the stability of the assembly flight.

C. PROOF OF THE RANGE OF THE PARAMETER λ OF CTFAP ALGORITHM

In the actual flight, the error of the trajectory following is smaller than $a\%(a = 1$ in the simulation of this paper),

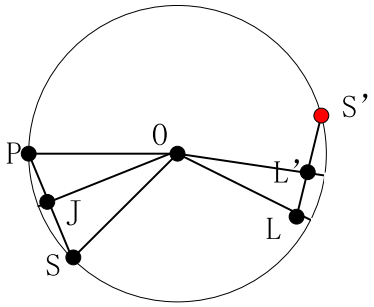

FIGURE 3. Schematic diagram of the CTFAP algorithm.

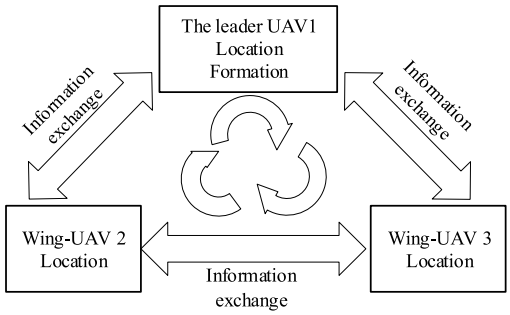

FIGURE 4. The schematic diagram of UAVs communication.

that is, the trajectory coincides without deviation. Due to the previous papers, the classical path following algorithm can make the UAV position error of preset circular trajectory less than $a\%$, but it is not stable. In Figure 3, when the UAV is near the point L of the circular trajectory (the error between the UAV and the circular trajectory is less than $a\%$), with the algorithm in Section II.B and the preset parameter λ, the point S' is solved to be the offset point in the circular trajectory of the UAV at this moment. LS' is the flying direction. With the knowledge of circle and triangle, the distance between the point L' in the line LS' and the circle can be solved. If the distance error from the point L' to the circle is less than $a\%$, the UAV can converge on the circular trajectory.

Assume that the UAV has already moved to the position which coincides with the track [20], [36], [37], how to ensure that the position of the UAV in the next moment is still coincident with the track? In Figure 3, the point P is the location of the UAV (the error between the UAV and the track is less than $a\%$). The point S is the offset point of the point P (There is an angle λ between the point S and the point P in the circle). d is the distance. V is speed of UAVs.

R is the radius of the circle. Formula (2-5) can be launched by the previous assumption $d \leq a\% * R$.

$$\left.\begin{array}{c} PS \leq 2\mathrm{R}\sqrt{1-(1-a\%)^2} \\ \lambda = 2\arcsin(\frac{PS}{2R}) \end{array}\right\} \Rightarrow \lambda \leq 2\arcsin(\sqrt{1-(1-a\%)^2} \quad (2\text{-}5)$$

Formula (2-6) can be launched by the limit of the UAV's speed.

$$\left.\begin{array}{c} PS \geq V * dt \\ \lambda = 2\arcsin(\frac{PS}{2R}) \end{array}\right\} \Rightarrow \lambda \geq 2\arcsin(\frac{\mathrm{V} * \mathrm{dt}}{2R}) \quad (2\text{-}6)$$

Formula (2-5) ensures that the flying path of the UAV is in the error range of the trajectory. Formula (2-6) ensures that the UAV cannot fly out of the trajectory, and ultimately ensures that the flying path of the UAV can converge to the circular trajectory. With formula (2-5), formula(2-6), speed V of the UAV, radius R of circular trajectory and distance error $a\%$, the best interval can be solved: ($[2\arcsin(\mathrm{V} * dt/2R), 2\arcsin(\sqrt{1-(1-a\%)^2}]$).

III. DMPC MODEL FOR TARGET FORMATION RECONSTRUCTION

After the multi-UAV formation completes assembly, it needs to efficiently move from the initial state to the specific formation state to complete the formation reconstruction under the constraints. UAV formations communicate their respective status information in real time through the self-organizing network. As Figure 4 shown, under the constraints information of the formation sent by the leader UAV, the rapid prototyping and the reconstruction of the formation are completed, forming the host-down mode (reconstructed from 'gable' to 'diamond'), and guide the UAV formation to the next mission site (target point).

UAV formations communicate their respective status information in real time through the self-organizing network. As Figure 4 shown, under the constraints information of the formation sent by the leader UAV, the rapid forming and the reconfiguration of the formation are completed, forming the host-down mode.

The leader UAV receives the command from the ground, which commands the leader UAV to guide the formation to form a specific formation such as: A formation and B formation, and to guide the multi-UAV formation to the next mission location (the target point). The wing-UAVs receive the position information and follow the leader UAV to the mission location. During the period, the wing-UAVs receive the formation information (the leader UAV sends the relative positions of the wing-UAVs to itself) to form a specific formation required by the ground command. The reconfiguration of the target formation begins when the assembly is completed on the circle trajectory.

A. DMPC FRAMEWORK OF THE MULTI-UAV FORMATION

During the reconfiguration of the multi-UAV formation, the dynamic characteristics of each UAV is decoupled. Its control structure can adopt the distributed model predictive control (DMPC) to complete the formation reconfiguration task by the interaction of their respective position states and the constraints [38]. Under the DMPC framework, each UAV has its own model predictive controller to solve the control domain and to select the control value.

Under the DMPC framework, each UAV has its own model predictive controller to solve the control domain and to select

the control value, the behaviors of n UAVs formation can be jointly described and solved by each UAV. Therefore, DMPC has been widely used in the research of the reconfiguration of the UAV formation [39]–[41]. The formation motion formula is expressed as formula (3-1):

$$f(\tilde{x}(k), \tilde{u}(k)) = \left[f_1(X_1(k), U_1(k))^T, \ldots, f_N(X_n(k), U_n(k))^T\right] \tag{3-1}$$

In formula (3-1), $\tilde{x}(k), \tilde{u}(k)$ are the vector of the total state and the control amount of the multi-UAV formation at the k moment. When the control input is known (that is, $\tilde{u}(0), \tilde{u}(1), \tilde{u}(2), \ldots, \tilde{u}(n), \tilde{x}(0)$ are given), the formation status at the $k = n * dt$ moment can be launched by formula (3-1).

Under the DMPC framework, the cost of the target formation reconfiguration of the n UAVs formation can be divided into the sum of each UAV's control, as shown in formula (3-2):

$$J(\tilde{x}(k), \tilde{u}(k)) = \sum_{i=1}^{N} J_i\left(\mathbf{X}_i^{\mathrm{N}}(k), \tilde{x}(k-1), \mathbf{X}^N(k-1)|, \mathbf{U}_{\mathrm{i}}^N(k)\right) \tag{3-2}$$

In formula (3-2), $X_i^{\mathrm{N}}(k)$ and $U_i^N(k)$ are the N-step-predicted state and control set of the i UAV at the k moment. $X^N(k-1)$ is the N-step-predictive state set for all UAVs in the formation at the k moment, as shown in formula (3-3):

$$\begin{aligned} \mathbf{X}_i^N(k) &= \{X_i(k|k), X_i(k+1|k), \ldots, X_i(k+N-1|k)\} \\ \mathbf{U}_i^N(k) &= \{U_i(k|k), U_i(k+1|k), \ldots, U_i(k+N-1|k)\} \\ X^N(k) &= \{X_1^N(k), X_2^N(k), \ldots, X_n^N(k)\} \end{aligned} \tag{3-3}$$

Under the DMPC framework, the overall reconfiguration problem of the formation can be simplified to n local optimization problems of individual UAV, as shown in formula (3-4):

$$\mathbf{u}_i(k) = \underset{U_i(k)}{arg\,min}\ J_i\left(\mathbf{X}_i^N(k), \mathbf{X}^N(k-1), \mathbf{U}_i^N(k)\right) \tag{3-4}$$

Formula (3-4) shows that under the framework of DMPC, the optimization in each time domain is only related to the status $X_i(k)$ and the control set $U_{\mathrm{i}}^N(k)$ of the either UAV, the state $\tilde{x}(k-1)$, the forecast information of all UAVs at last moment received by the network. The optimization goal range is reduced because only $U_{\mathrm{i}}^N(k)$ needs to be solved and the efficiency of optimization solution is improved.

B. THE COST FUNCTION OF FORMATION RECONFIGURATION UNDER DMPC FRAMEWORK

This paper divides the constraints into the constraint of the target formation reconstructed status, the constraint of the target position approaching and the constraint of the in-team collision prevention [42], [43]. Therefore, the cost function of the UAV formation is divided into the following three parts, the constraint function is defined as follows:

1) THE COST FUNCTION OF RECONSTRUCTED STATE

For complete the formation reconfiguration with high efficiency, the cost function of reconstructed state is selected as formula (3-5)

$$\begin{aligned} J_{iF}(k) = &(X_i(k) - X_{if}(k) \\ &+ \sum_{0}^{N-2} \alpha * \left\|X_i(k+q|k) - X_{ip}(k+q|k-1)\right\|^2) \\ &+ \sum_{q=1}^{q=N-2} \beta * \|U_i(k+q|k)\|^2 \end{aligned} \tag{3-5}$$

In formula (16), the explanation of $X_{if}(k)$ and $X_{\mathrm{ip}}(k+m|k-1)$ is shown as formula (3-6):

$$\begin{aligned} X_{if}(k) &= X_1(k) + L_i \\ X_{ip}(k+m|k-1) &= X_1(k+m|k-1) + L_i; m \in (1, N-2) \end{aligned} \tag{3-6}$$

In formula (3-6), L_i is the relative position information of the either UAV about the leader. $X_{if}(k)$ is the expected status of the either UAV at the k moment. $X_{ip}(k+m|k-1)$ is the current expected state of any UAV based on the prediction of k-1 time. The previous item guarantees that the formation can reach its target formation status, and the last item guarantees the high control efficiency.

2) THE COST FUNCTION OF TARGET APPROACHING

For make the UAV formation reach the mission target point with higher efficiency, the heading of the UAV should be the direction of the mission point. The cost function of target approaching is taken as formula (3-7):

$$\begin{aligned} J_{id}(k) = &\sum_{q=0}^{q=N-1} r_q \left\|\chi_i(k+q|k) - angle_{id}(k+q|k)\right\|^2 \\ &+ \sum_{q=0}^{q=N-1} h_q \left\|V_i(k+q|k) - V_0\right\|^2 \end{aligned} \tag{3-7}$$

In formula (3-7), $angle_{id}(k+q|k)$ is the angle between the UAV and the target point at the N-step-prediction. V_0 is the expected speed. The previous item guarantees the direction of the formation, and the last item guarantees the speed of the formation.

3) THE COST FUNCTION OF THE IN-TEAM COLLISION

For prevent collisions within the team during the formation forming, the safe distance is set. The cost function of the in-team collision is shown as formula (3-8):

$$\begin{aligned} J_{ic}(k) = &\sum_{\substack{j=1 \\ j\neq i}}^{n} (len(X_i(k), X_j(k)) + \sum_{m=1}^{N-2} len(X_i(k+m|k), \\ &\times X_j(k+m|k-1))) \end{aligned} \tag{3-8}$$

The function in formula (3-8) is described in formula (3-9):

$$len(X_i(k), X_j(k)) = \begin{cases} \eta(2D - d_{ij}), dij < 2D \\ 0, \text{others} \end{cases} \quad (3\text{-}9)$$

In formula (3-9), d_{ij} is the Euclidean distance between the either UAV and the either UAV at the k moment. D is the collision radius of the UAV. The previous item guarantees that there will be no collision between the UAV team at the current moment, and the latter item will predict the future collision cost.

In summary, the total cost function of UAV formation is given in formula (3-10):

$$\begin{aligned} J_i(k) = & \left\| x_i(k+N|k) - x_{if} \right\|^2 \\ & + \sum_{q=0}^{q=N-1} \left(\left\| x_i(k+q|k) - x_{if} \right\|^2 + \left\| u_i(k+q|k) \right\|^2 \right) \\ & + \sum_{q=0}^{q=N-1} r_q \left\| \chi_i(k+q|k) - angle_{id}(k+q|k) \right\|^2 \\ & + \sum_{q=0}^{q=N-1} h_q \left\| V_i(k+q|k) - V_0 \right\|^2 \\ & + \sum_{\substack{j=1 \\ j \neq i}}^{n} (len(X_i(k), X_j(k)) \\ & + \sum_{m=1}^{N-2} len(X_i(k+m|k), X_j(k+m|k-1))) \end{aligned} \quad (3\text{-}10)$$

So far, this paper has completely built the multi-UAV formation mathematical model under the DMPC framework.

IV. IMPROVED DE ALGORITHM FOR SOLVING DMPC MODEL

For the DMPC model with the above cost function, the researchers propose many optimization algorithms such as PSO and DE algorithm. Among them, the differential evolution algorithm has the strong global search ability and the fast convergence ability. However, the traditional DE algorithm is slow in iteration. The main reason is that the population of each iteration is randomly generated and does not inherit the result of the previous calculation of the framework or formation model. This paper inherits the prediction information of the DMPC model to improve the differential evolution algorithm named as Pre-DMPC-DE algorithm, which increases the optimized population operation and greatly improves the efficiency of the solution.

A. PRE-DMPC-DE ALGORITHM FOR DMPC MODEL

Under the DMPC framework, the forming problem of the whole UAV formation can be differentiated into the problem of optimizing the control quantity set $U_i^N(K)$ of n relatively independent UAVs. Pre-DMPC-DE algorithm uses the N-step predictive control set $U_i^N(K)$ as the individual in the DE algorithm, randomly generates M sets of predictive control quantities as the population of the DE algorithm, and uses the formation cost function as the individual evaluation function of the DE algorithm.

Optimization of the Pre-DMPC-DE is that:

1) M represents the size of the population. The population is Randomly initialized in the feasible space for solving the problem. $G^0 = \{g_1^0, g_2^0, \ldots, g_M^0\}$ (0 indicates the number of the iteration). $g_j^0 = U_i(k)$ (That is

$$\begin{aligned} g_j^0 = & \{u_i(k|k), u_i(k+1|k), \ldots, u_i(k+N-1|k)\}, \\ & \times i \in [1, n], j \in [1, M]). \end{aligned}$$

2) After loop iterations of mutation, crossover and selection operations, the best individual g_{best}^t are obtained in the population. g_{best}^t is brought in formula (3-11) to get the optimized individual g_{new}^0 at the next moment. That is the increased optimizing population operation, which is shown in formula (3-11).

$$\begin{aligned} g_{new}^0 &= g_{best}^t * A \\ \mathrm{G}_{new}^0 &= G^0 \cup \left[\mathrm{g}_{new}^0 \right] \\ A &= \begin{bmatrix} 0 & 0 \\ E & 0 \end{bmatrix} \end{aligned} \quad (3\text{-}11)$$

In the DMPC framework, the first part control quantities $u_i(k|k)$ of $U_i^N(K)$ control the next movement of the UAV, and the current optimization solution will discard the set of the remaining control quantities ($\{u_i(k+1|k), \ldots, u_i(k+N-1|k)\}$). The set of the remaining control quantities has high adaptability for the evaluation function, which has the prior knowledge at the k moment. Therefore, this paper uses this information on the Pre-DMPC-DE algorithm to optimize the population, and to generate excellent individuals ($\{u_i(k+1|k), \ldots, u_i(k+N-1|k), u_i(k+N|k+1)\}$) with excellent genes for the next moment. The Pre-DMPC-DE algorithm accelerates the process of population optimization by the cross-evolution of good individuals and random individuals to solve the optimal control set $U_i^N(k)$ with fewer iterations.

B. PROPOSED FORMATION SOLUTION BASED ON DMPC BY PRE-DMPC-DE

As described above and the flow chart shown in Figure 5, a solution of structure reconstruction Pre-DMPC-DE algorithm is proposed. The steps are as follows:

Step 1: At time k, all the wing UAVs send their own status information $X_i^N(k-1)$ to the leader UAV through the communication between the formations, and the leader communicates the status information of the unmanned aerial vehicles at the previous moment through the communication between the formations $X^N(k-1)$. And the formation information L_i is sent to all slaves. The optimal control quantity $U_i^N(k)$ is used to perform the optimized population operation in the Pre-DMPC-DE algorithm given in Section IV(A) of the initial population in Figure 5,

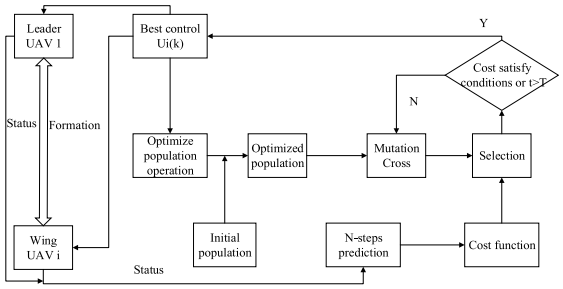

FIGURE 5. The flow chart of the forming problem of the formation.

and finally the optimized population unique to the wing UAV is generated. Go to step 2;

Step 2: The proposed algorithm uses the mutation operation and crossover operation in the Pre-DMPC-DE algorithm to evolve the individual g_j^t in the optimized population of the wing UAV; The DMPC framework in section III(A) and the cost function proposed in section III are defined as an evaluation model and evaluation function, all evolutionary individuals are evaluated to obtain individual evaluation values, and whether the individual evolves is determined by the selection operation, if the evolution fails, it replace its parent. As shown in Figure 5, the population evolution of step 2 is repeated until the evaluation value of the optimal individual satisfies the condition, or the number of iterations of step 2 exceeds the setting of the algorithm (the maximum number of iterations is set to 500), and the optimized population is evaluated. The highest value individual g_{best}^t. Go to step 3;

Step 3: It can be known from section IV(A) that the individual in the population is the control quantity set of the wing UAV, the optimal individual g_{best}^t is the optimal control quantity set $U_i^N(k-1)$ of the slave machine either UAV at the k-1 moment. This optimal control amount is transmitted to step 1, and the next optimal control amount is obtained according to formula 9, applied to the flight of the wing UAV, and the wing UAV reaches a new state. Return to step 1.

The flow chart for solving the forming problem of the multi-UAV formation under the DMPC framework is shown in Figure 5:

C. CONVERGENCE PROOF OF PRE-DMPC-DE ALGORITHM FOR DMPC

Theorem 1: The evaluation value of the Pre-DMPC-DE algorithm does not increase as the number of iterations increases.

Proof: The selection operation of the DE algorithm shows that the operation is performed only when the cost is reduced, so the algorithm generation value does not increase as the number of iterations increases.

Theorem 2: The population in the Pre-DMPC-DE algorithm is the Markov chain.

Proof: All operations of the DE algorithm are independent of the number of iterations, so the $t+1$ generation X^{t+1} of the algorithm is only related to the t generation X^t. Therefore, the population is a Markov chain. Its transition probability is formula (3-12):

$$\begin{aligned} &P(\mathbf{X}(t+1)=\mathbf{Y}|\mathbf{X}(t)=\mathbf{X}) \\ &\quad=\begin{cases}\prod_{i=1}^{\mathrm{N}} P\left(T(\mathbf{X}(t))_i=x_i(t+1)\right), \textit{restriction} \\ 0, \textit{other}\end{cases} \\ &\quad\texttt{restriction}: \exists i_x, i_y \in [1,M], s.\mathrm{t}.F\left(x_{ix}\right) \\ &\quad=F_{\min}(\mathbf{X}), F\left(y_{iy}\right)=F_{\min}(\mathbf{Y}) \end{aligned} \tag{3-12}$$

In formula (3-12), $F_{\min}(X)$ is the minimum cost of the population $G=[g_1, g_2, \ldots, g_n]$.

Theorem 3: The population G of the Pre-DMPC-DE algorithm converges to the satisfactory species cluster V $*$ in the solution space with the probability 1, as shown in formula (3-13):

$$\lim_{t\to\infty} P(X(t)\in V^*|X(0)=X_0)=1 \tag{3-13}$$

Proof: Let x $*$ be the optimal solution of the cost function. $P(X, Y)$ Expresses $P(X(t+1)=Y|X(t)=X)$. Formula (3-22) introduces the following two points:

(1). If $X, Y \in V^*$, then $P(X, Y)>0, P(Y, X)>0$. That is, two states interoperate $X<->Y$;

(2). If $X \in V^*, Y \in V^*$, then $P(X, Y)=0$. That is, two states don't interoperate. X is not available to Y.

V $*$ is an aperiodic irreducible closed set, so there is formula (3-13) for any initial state:

$$\lim_{t\to\infty} P\left(\mathbf{X}(t)=\mathbf{Y}/\mathbf{X}(0)=\mathbf{X}_o\right)=\begin{cases}\pi(\mathbf{Y}), \mathbf{Y}\in V^* \\ 0, \mathbf{Y}\notin V^\star\end{cases} \tag{3-14}$$

The initial state is bound to enter a satisfactory species group. Its ultimate probability satisfies the distribution π (Y), that is formula (3-15):

$$\lim_{t\to\infty} P\left(\mathbf{X}(t)\in V^{\mathring{a}}|\mathbf{X}(0)=\mathbf{X}_0\right)=1 \tag{3-15}$$

Therefore, the Pre-DMPC-DE algorithm can solve the formation reconfiguration problem of the DMPC model, and the algorithm is convergent.

V. THE ANALYSIS OF THE SIMULATION EXPERIMENTS

This paper carries out the simulation verification of the algorithm performance with the simulation software Matlab2019 and Intel 2.8G CPU with 16GB Memory. Simulation 1 is a simulation of the circular assembly with the circle trajectory following algorithm, which has five UAVs. It verified the effectiveness of the adaptive parameters and the rapid stability of the assembly. For verify the excellent performance of the proposed Pre-DMPC-DE algorithm, simulation 2 gave experimental comparison of different optimization algorithms. Differential Evolution (DE) [19], [20], genetic algorithm (GA) [21], particle swarm optimization- (PSO) [22], [23], genetic learning particle

TABLE 1. Constraint parameters of UAVs.

	Speed m/s	Heading	Acceleration m*s^{-2}
Min	0	-180^0	-5
Max	100	-180^0	5
	Pitch	Heading-velocity	Pitch-Velocity
Min	45^0	-36^0	-15^0
Max	135^0	36^0	15^0

TABLE 2. Initial kinematic parameters of UAVs.

	Departure Location	Departure time s
UAV1	(0,0,0)	1
UAV2	(0,0,0)	2
UAV3	(0,0,0)	3
UAV4	(0,0,0)	4
UAV5	(0,0,0)	5
	Expected Speed m*s^{-1}	Max speed m*s^{-1}
UAV1	60	70
UAV2	60	70
UAV3	60	70
UAV4	60	70
UAV5	60	70

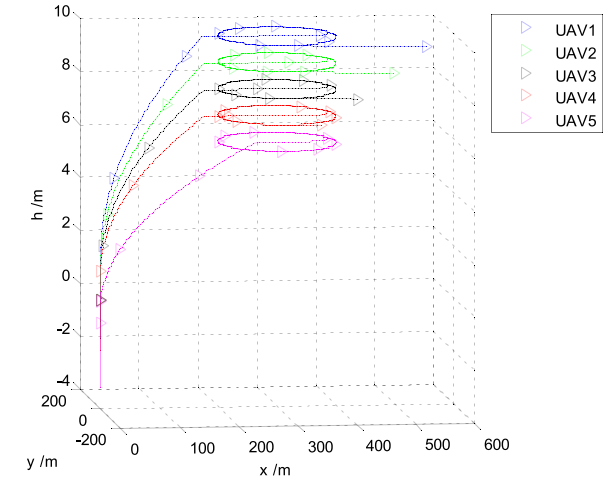

(a) Three-dimensional flying diagram of the circular trajectory formation taking off

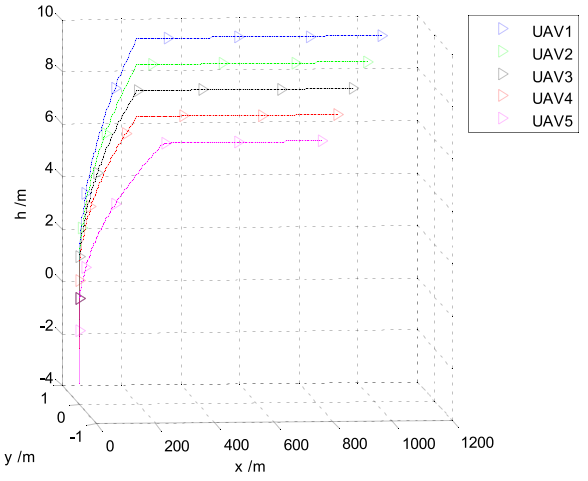

(b) Three-dimensional flying diagram of the line formation take-off

FIGURE 6. Comparison of the circular trajectory take-off and the straight-line take-off.

swarm optimization (GLPSO) [24], historical and heuristic-based adaptive differential evolution (HHDE) [25] and Pre-DEMPC-DE algorithms were used to execute the simulation of multi-UAV formation forming and reconfiguration. For verify the overall effectiveness of CTFAP and Pre-DMPC-DE algorithms, simulation 3 used simultaneously the proposed CTFAP and Pre-DMPC-DE algorithms to make a simulation of multi-UAV assembly and formation reconfiguration.

These experiments stipulate that there is no communication delay between the UAVs in the formation; the speed and heading angle of the UAV are not affected by any other factors. The fixed-wing UAV is selected in this experiment. The parameters are shown in Table 1.

Simulation 1: Verify the functionality of the circle trajectory following assembly algorithm in this article and the advantages of the algorithm compared with normal line assembly.

Simulation scenario: Five UAVs take off in sequence at 1 s intervals. The assembly method adopts the CTFAP algorithm and the linear formation algorithm which commonly used in practice. The initial parameters of the UAV formation members are shown in Table 2. UAV 1-5 refers to the UAV number, of which No. 1 is the leader. The three parameters of take-off position refer to the East direction, the north direction and the height from the ground in the Northeast celestial coordinate system, with the take-off point as the origin. Expected speed refers to the final mission execution speed of UAV formation, and maximum speed refers to the maximum flight speed of each UAV formation.

Figure 6 is a three-dimensional flying diagram showing the circular trajectory assembly and formation reconfiguration and the linearly assembly and formation forming. In order to clearly indicate the trajectory status of different UAVs and avoid overlapping trajectories at the same altitude, Figure 6(a) makes concentric circle trajectories at different altitudes for formation members UAV1-UAV5. The triangular arrows in the Figure 6 indicate the location of all UAVs every 10 seconds. In the following Figure 12(b), we can find that

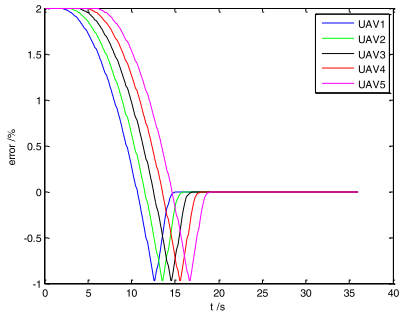

FIGURE 7. Trajectory offset error of circular trajectory assembly flight.

the 2-D circular trajectory diagram shows that the formation assembly of 5 UAVs are in the same circular orbit.

In Figure 6(a), the rise of the left curve indicates the climbing phase of the UAVs, and the circular curve represents the track where the multi-UAV formation is assembling. When the circular track assembly is completed, the distance of the leader UAV (UAV1) from the take-off point is 400 meters. The arrow line on the right indicate that the UAVs fly out of the circular assembly and complete the formation reconfiguration and forming. Figure 6(b) is the 3-D flying diagram of the UAVs' straight-line assembly. As the figure shows, these UAV gradually form an assembly of equal space. However, when the assembly formation is completed, the leader UAV is at the 1100 meters of the x-axis, which is far bigger than the 400 meters of the circle trajectory assembly.

Figure 7 shows the offset error of circular trajectory assembly flying of the formation. The ballistic error value in Figure 7 is the ratio of the shortest distance from the UAV to the circular trajectory to the radius of the circular trajectory (100m). The smaller the error is, the better the coincidence degree between the UAV trajectory and the predetermined circle trajectory is. When the error value is 0, it means the complete coincidence. Figure 7 shows that in the period from 0 s to 17 s on the t-axis (the axis of the time), the error values of the five UAV are decreasing. Meanwhile, the five UAV are all in the acceleration phase, flying from the take-off point to the center of the circular track. Between 14s and 17s, line segments of each color that reach the lowest point and bounce, indicate that these UAVs passed the center of the circular trajectory and began to track the circular trajectory. When the error values of all UAVs stabilize in a straight line, all UAVs stably track circular trajectory with the error less than the assumption (1%). That is, the error distance of all UAVs is less then 1 meter.

Figure 8 is the diagram of the distance between UAVs of two assembly algorithms and formation forming. The t-axis is the time axis, indicating the time point after takeoff of formation, and the distance axis is the distance between wing UAVs and leader UAV. The distance is the length between the wing-UAV (UAV2-UAV5) and the leader UAV (UAV1). As shown in Figure 8(a), the distance of UAV5 reaches the maximum in the crest, which is 200 meters. The UAV2-UAV5 curve represents the distance between the

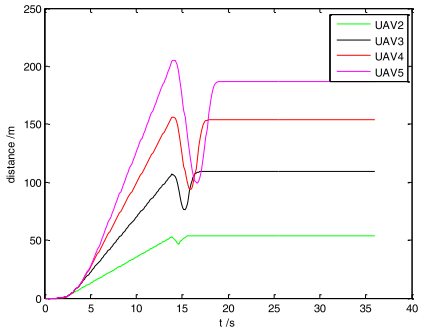

(a) Diagram of the circular assembly and formation

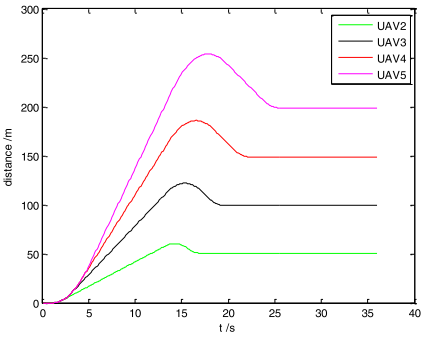

(b) Diagram of the linear assembly and formation

FIGURE 8. Comparison of the circular formation and the beeline formation.

TABLE 3. Comparison of formation forming time and distance.

algorithm	Average of stable time /s	distance/m
Circular assembly and formation	18	600
Circular assembly and formation	23	1022

current UAV and UAV1.So, the max distance of the CTFAP algorithm is 200 meters at t = 13s. Figure 8(a) The straight line on the right indicates that the formation is stable, and the distance is stable at the set value of the formation. The distance of UAV5 in Figure 8(b) is 250 meters at t = 18s, so the max distance of the linear assembly algorithm is 250 meters. The circular assembly algorithm is 25% smaller than the linear assembly algorithm in the max distance. The experimental data shows that the circular assembly algorithm consumes less communication performance than the linear assembly formation algorithm.

Table 3 shows the numerical results of formation forming time according to the all lines stable time in Figure 8. The results show that compared with the linear combination algorithm, the stability time of CTFAP algorithm in this paper is shortened by 21%, and the distance from takeoff to formation point is shortened by 41%, which can complete formation combination and formation in a small area.

TABLE 4. Parameters of algorithms.

Algorithm	parameters
DE	Variation probability 0.6, Cross probability 0.6
GA	Cross probability 0.3, Variation probability 0.008
PSO	Weight 1, Learning factor 0.49445
GLPSO	Weight 1, Learning factor 0.7298
HHDE	Strategy factor 0.2, Variation factor 0.1, Cross factor 0.7

TABLE 5. Model parameter.

Sampling period dt	Cost factor α，β, r, h	
0.5	100,10,50,50	
Step size	Simulation period T	Destination
5	50 s	(5000,0)

Simulation 2: Comparison of the performance of the multi-UAV formation reconfiguration algorithm with different algorithm. The average iteration times, completion time, reconstruction trajectory and reconstruction trajectory errors are compared. GLPSO, HHDA and DMPC-DE algorithms are applied in these simulations. Assembly and formation reconfiguration, and the average number of iterations in the reconstruction process is compared with the experimental results, and the reconstruction time, the reconstruction track and the reconstruction track error are all given in this section. The initial population is 30 and the maximum number of iterations is 300. The parameters of the above algorithms are shown in Table 4. The model parameters are shown in Table 5. The initial parameters of the multi-UAV formation are shown in Table 6: The algorithm parameters in the following table can be explained by the formula in the paper. For example, the mutation parameters and crossover probability in DE algorithm are the parameters in formula 12 of original DE algorithm. The parameters in Table 4 below are all the same. Sampling period, prediction step, cost coefficient and target point in model parameters are all mentioned in the formula in Section III. The initial parameters of UAV are set by itself. The three parameters of the initial position refer to the East direction, the north direction and the height from the ground in the Northeast celestial coordinate system, respectively, with the take-off point as the origin. The relative position is the position error of slave position relative to long position in reconstructed formation. Heading angle is a parameter in UAV mathematical model, which is explained in Section II(A). Expected speed refers to the final mission execution speed of UAV formation, and maximum speed refers to the maximum flight speed of each UAV formation.

TABLE 6. Initial kinematic parameters of UAVs.

UAV	Location	Heading	Expected position
UAV1	(0，0，60)	0°	(0,0,0)
UAV2	(-100，100，60)	0°	(-50,50,0)
UAV3	(-100，100，60)	0°	(-50,50,0)
UAV4	(-200，200，60)	0°	(-100,100,0)
UAV5	(-200，-200，60)	0°	(-100，-100,0)
UAV	Expected speed $m*s^{-1}$		Max speed $m*s^{-1}$
UAV1	80		80
UAV2	80		90
UAV3	80		90
UAV4	80		90
UAV5	80		90

In Figure 9(a), the x-axis represents the iteration number axis and the y-axis represents the cost value axis. The relationship between the value of each algorithm and the number of iterations per iteration is represented by two axes. In Figure 9(b), x axis is the axis of the algorithm, and the y axis is the average number of iterations (the average number of iterations each time the optimal solution is obtained). The two axes jointly represent the average converge speed of each algorithm. Figure 9(a) shows the cost descending sequence of the above different algorithms at 45s. Figure 9(b) shows the comparison of the improved DE algorithm (Pre-DMPC-DE) and other algorithms on the average number of iterations. The green line in Figure 9(a) represents the cost value drop curve of Pre-DMPC-DE algorithm, which is below the curve of all other algorithms, which shows that the cost value of this algorithm is generally lower than that of other algorithms. In the first few seconds, the gradient of curve drop is large, and the cost value is dropping faster than other algorithms. Figure 9(a) shows that Pre-DMPC-DE algorithm can achieve rapid cost reduction with fewer iterations. It shows that the improved algorithm has a strong iterative optimization ability and quickly completes the optimization solution for this control quantity set. The comparison of the histogram in Figure 9(b) shows that the average number of iterations of the classical DE algorithm is nearly 200, while the other improved algorithms is nearly 170 times. But the Pre-DMPC-DE algorithm proposed in this paper has an average number of iterations which is less than 150 times. The improved DE algorithm reduces the number of iterations by 16% $\sim$ 30%, which greatly saves time and resource consumption of the computation in solving the problem of the UAV formation control.

For further verify the advantages of the Pre-DMPC-DE algorithm, simulation experiments of these multi-UAV

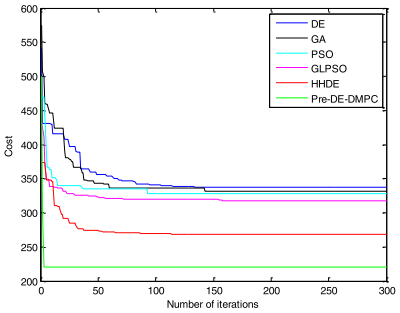

(a)Decreasing diagram of the cost with iterations

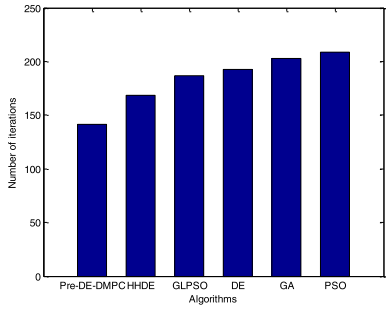

(b)Histogram of average iterations of all algorithms

FIGURE 9. Cost diagram and histogram of iterations.

formations reconfiguration are carried out, which respectively have 5, 10, 20 and 40 UAVs. The total calculation time from take-off to the formation forming is shown in Table 7. In this simulation, the time performance of the algorithm is investigated at the scale of 5, 10, 20 and 40 UAVs and the formation aggregates from disordered state to formation flying state in random initial state (this process does not include circular aggregation, but only further verifies the reconstruction algorithm).The experimental results show that the Pre-DMPC-DE algorithm has obvious advantages in the calculation time in the case of the continuous expansion of the UAV formation. From Table 7, we can see that the Pre-DMPC-DE algorithm proposed in this paper consumes more than 18% less than all the other algorithms in the total time of UAV reconstruction calculation.

Figure 10 is the comparison of the trajectory maps of the five UAVs with afferent algorithm (reconstructed from 'gable' to 'diamond'). The small triangle with each color represents a UAV. Among them, the UAV1 is the leader UAV. These UAVs' position is displayed every 5 seconds. Figure 10(a) is the output trajectory of the Pre-DMPC-DE algorithm proposed in this paper. The entire trajectory is smooth and does not produce large trajectory oscillations. Five triangles form gable formation at the left, then 11th second of the flight, the diamond formation is basically formed. The UAV formation is stable before the 16th second, as shown at the right of the Figure 10(a), five triangles form the

TABLE 7. Results of multiple UAVs formation reconfiguration time experiments (millisecond).

5 UAVs	10 UAVs	20 UAVs	40 UAVs
Pre-DMPC-DE	51	91	201	390
HHDE	61	112	252	482
GLPSO	103	209	427	828
DE	82	206	344	653
PSO	92	174	383	733
GA	71	134	301	587

diamond formation. Figure 10(b) is the trajectory of the HHDE algorithm. At the 11th second of the flight, the formation is basically formed. The UAV formation is stable before the 16th second. However, the trajectory of the UAV5 produces a slight turbulence. Figure 10(c) is the trajectory of the GLPSO algorithm. At the 11th second of the flight, the formation is basically formed. The UAV formation is stable before the 16th second. However, the trajectory of the UAV4 produces a turbulence, and the flying distance of the UAV4 is far. Figure 10(d) is the trajectory of the DE algorithm. At the 11th second of the flight, the formation is basically formed. The UAV formation is stable before the 16 second. Figure 10(e) is the trajectory of the PSO algorithm. In figure 10(e), the trajectory of the UAV4 produced a large shock, and it was before the 21th second that the formation reconfiguration is completed. Figure 10(f) is the trajectory diagram of the GA algorithm. The trajectory of the UAV formation has undergone a large oscillation. After the 31th second, the formation is basically stable, and the reconfiguration of the formation is completed. So the proposed Pre-DMPC-DE algorithm achieve great performance on rapid formation forming and reconfiguration. Compared with the smoothing of the trajectory and the flight time of the reconstructed formation, the Figure 10(a) of the Pre-DMPC-DE algorithm in this paper is better than that of the other algorithms. It is further shown that the proposed algorithm is superior to other algorithms.

Figure 11 is the comparison of the sum of the trajectory error of the above algorithms. The error value is defined as the distance between the position of the wing-UAV and the position transmitted by the leader UAV. The sum of error is the sum of the trajectory error of all wing-UAVs. It can be seen from Figure 11 that the Pre-DMPC-DE algorithm proposed in this paper has the smallest trajectory error and the fast falling speed, and the sum of error is minimum at the same time. In the purple PSO curves, the error curves rebounding at some time points $t = 16$ indicates that a UAV has a sharp shock at this moment. The proposed Pre-DMPC-DE algorithm only has one rebound. It indicates the stability of the convergence of this Pre-DMPC-DE algorithm is better

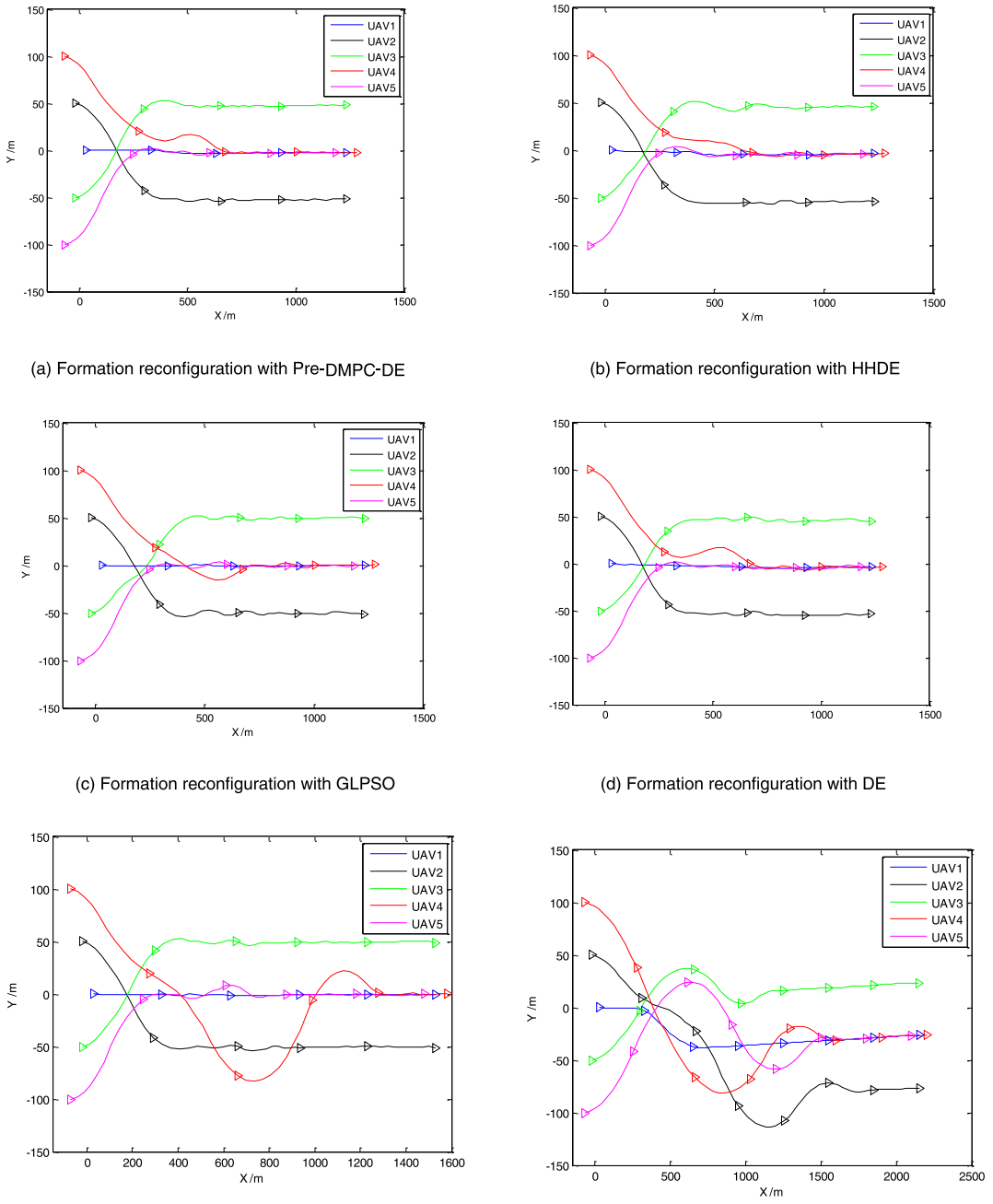

(a) Formation reconfiguration with Pre-DMPC-DE

(b) Formation reconfiguration with HHDE

(c) Formation reconfiguration with GLPSO

(d) Formation reconfiguration with DE

(e) Formation reconfiguration with PSO

(f) Formation reconfiguration with GA

FIGURE 10. **Comparison of trajectory of the multi-UAV formation reconfiguration with different algorithms.**

than other algorithms. Assume that the trajectory error of the UAV formation is 30 meters, that is, the special formation is basically formed. From Figure 11 we can see that the Pre-DMPC-DE algorithm is completed at the 12.5 second, while the remaining other algorithms form the basic formation at least after the 14 second. The comparison of these algorithms from Figure 10 and Figure 11 shows that: Pre-DMPC-DE algorithm is superior to other algorithms in both reconfiguration speed (in time) and accuracy (in oscillation).

Simulation 3: The simulation of the complete process from the departure to the formation reconfiguration. In this simulation, the accuracy, flight time consumption and flight distance consumption of the circular formation take-off algorithm and UAV formation reconstruction algorithm proposed in this paper are adopted. Five drones take off at one second intervals. The UAVs would assemble in the form of the circular over the airport and eventually fly out of the airport in gable formation. The Pre-DMPC-DE algorithm is used to

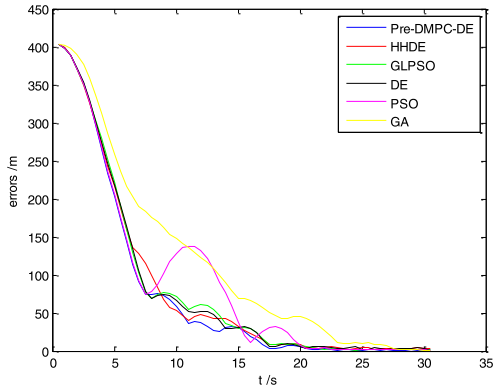

FIGURE 11. Comparison of the trajectory error of each algorithm.

TABLE 8. Model parameter.

Sampling period dt	Step size	Cost factor α，β, r, h
0.5	5	100,10,10,1
Simulation period T		Destination
85s		（5000,0）

TABLE 9. Initial kinematic parameters of UAVs.

UAV	Location	departure time	Expected position
UAV1	(0,0,0)	1	(0，0，0)
UAV2	(0,0,0)	2	(-50，50，0)
UAV3	(0,0,0)	3	(-50，-50，0)
UAV4	(0,0,0)	4	(-100，100，0)
UAV5	(0,0,0)	5	(-100，-100，0)
UAV	Expected speed m*s^{-1}		Max speed m*s^{-1}
UAV1	60		60
UAV2	60		70
UAV3	60		70
UAV4	60		70
UAV5	60		70

start the reconfiguration of the multi-UAV formation and the cruising of the target point. In the improved DE algorithm, the initial population is 30 and the maximum number of iterations is 300. The parameters of the DMPC are shown in Table 8. The relevant parameters of the UAVs are shown in Table 9. Table 8 sampling period, prediction step length, cost coefficient and target point in model parameters are given in the formula in Section III. The initial parameters of the UAVs of Table 9 are set. The three parameters of the take-off position refer to the east, the north and the height of the

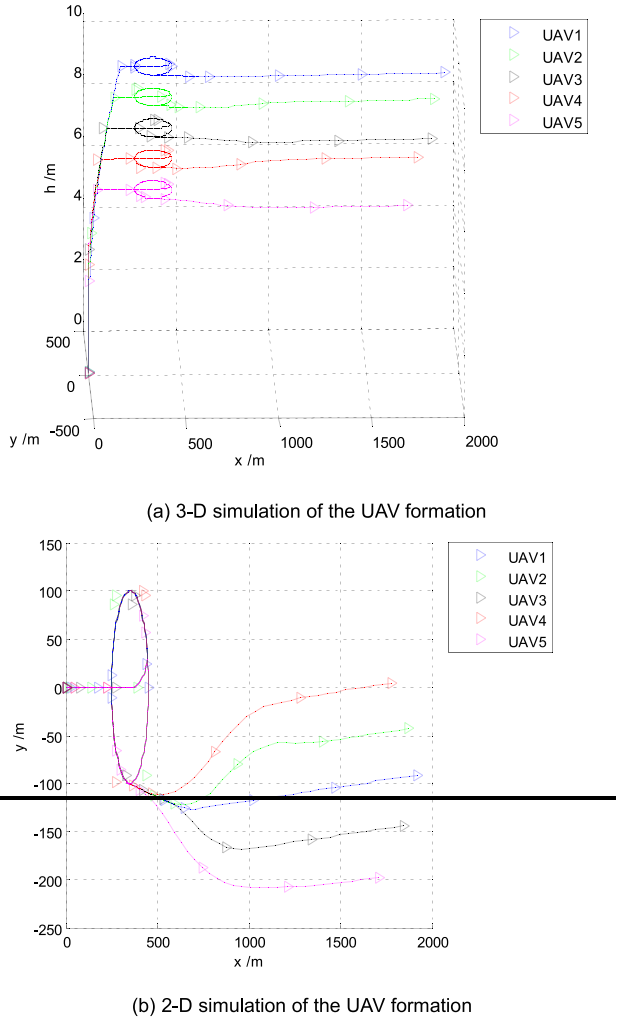

(a) 3-D simulation of the UAV formation

(b) 2-D simulation of the UAV formation

FIGURE 12. Track diagram of the formation from departure to reconfiguration.

ground in the north-east coordinate system, respectively, and taking the take-off point as the origin. The relative position is the position error of the slave position relative to the leader position in the reconstructed formation. The desired speed refers to the flight speed of the final mission of the UAV formation; the maximum speed refers to the maximum flight speed of each UAV.

Figure 12 is the 3-D and 2-D simulation results diagram of the multi-UAV formation from the departure to the formation reconfiguration. It can be seen from Figure 12(a) that the UAV formation takes off from the origin and makes a circular flying around the 300 meters diameter to the x-axis. All UAVs form the circular assembly on the circular trajectory, then the UAV assembly formation fly out of the circular trajectory at 500 meters to the X-axis direction. The formation enters the reconfiguration and forming stage and flies to the target point (5000,0). From Figure 12(b), it can be found that when the leader UAV (UAV1) reaches the 1500 meters at the x-axis, the UAV formation has basically completed the formation reconfiguration task. The three UAVs have the

same height (10 meters). For distinguish these flight paths in the three-dimensional diagram, the altitude of the subsequent UAVs was successively reduced by 1 meter. The experimental results show that the UAV formation correctly and accurately complete the task of the formation take-off, the formation reconfiguration and flying to the target location, which proves the correctness of the two algorithms proposed in this paper. The proposed cascade algorithm adopts the take-off mode of circular formation in this paper, which inherits the advantages of short takeoff distance and short flight time, reduces the time and space consumption of UAV formation. In addition, the reconstruction algorithm in this paper improves the calculation time in the process of UAV formation and reconstruction. Therefore, the cascade algorithm in this paper optimizes the time and space consumption of the previous algorithm in the process of UAV formation from take-off to formation.

VI. CONCLUSION

In this paper, the circle trajectory following assembly algorithm with adaptive parameters is applied to control the multi-UAV form the circular assembly formation. It reduces the inter-UAV distance of the formation, reduces the communication consumption and provides a new method for the fixed-wing UAV formation with the asynchronous takeoff way. We also propose an improved DE algorithm (Pre-DMPC-DE) based on the predictive information of DMPC for the rapid forming of the UAV formation. Compared with classical GA, DE, PSO, new GLPSO and HHDE algorithms, the results show that the improved algorithm improves the iterative rate and reduces the computation consumption with the better convergence ability of the UAV formation. Experimental results prove the feasibility of using the proposed algorithms in the process from take-off to formation forming task.

The cascade algorithm in this paper is suitable for sites with few runways and can't take off at the same time when UAV formation flies. This is true of most drone sites today, where the number of runways is smaller than the number of drones in formations. The number of UAV formations in this paper is still relatively small, and hundreds of UAV formations may complete the task in the future. How to use circular formation takeoff algorithm in the case of multiple aircraft taking off at the same time, and to ensure the mutual safety of aircraft is our next step subject to study and solve.

REFERENCES

[1] E. Besada-Portas, L. de la Torre, J. M. de la Cruz, and B. de Andrés-Toro, "Evolutionary trajectory planner for multiple UAVs in realistic scenarios," *IEEE Trans. Robot.*, vol. 26, no. 4, pp. 619–634, Aug. 2010.

[2] C. Sun, Y.-C. Liu, D. Grymin, and R. Dai, "Two approaches for path planning of unmanned aerial vehicles with avoidance zones," *J. Guid., Control, Dyn.*, vol. 40, no. 8, pp. 2076–2083, 2017.

[3] J. Zhang, J. Yan, P. Zhang, and X. Kong, "Collision avoidance in fixed-wing UAV formation flight based on a consensus control algorithm," *IEEE Access*, vol. 6, pp. 43672–43682, 2018.

[4] N. Wen, X. Su, L. Zhao, Y. Zhang, and P. Ma, "Online UAV path planning in uncertain and hostile environments," *Int. J. Mach. Learn. Cybern.*, vol. 8, no. 2, pp. 469–487, 2017.

[5] M. Radmanesh and M. Kumar, "Flight formation of UAVs in presence of moving obstacles using fast-dynamic mixed integer linear programming," *Aerosp. Sci. Technol.*, vol. 50, pp. 149–160, Mar. 2016.

[6] O. Cetin and G. Yilmaz, "Real-time autonomous UAV formation flight with collision and obstacle avoidance in unknown environment," *J. Intell. Robot, Syst.*, vol. 84, nos. 1–4, pp. 415–433, 2016.

[7] J. Zhang, J. Yan, and P. Zhang, "Fixed-wing UAV formation control design with collision avoidance based on an improved artificial potential field," *IEEE Access*, vol. 6, pp. 78342–78351, 2018.

[8] D. Lee, S. Kim, and J. Suk, "Formation flight of unmanned aerial vehicles using track guidance," *Aerosp. Sci. Technol.*, vol. 76, pp. 412–420, May 2018.

[9] Y. Zhou, G. Jiang, N. Cao, and F. Zhou, "Distributed multi-UAV formation control based on sliding mode method," *Inf. Control*, vol. 47, no. 3, pp. 306–313, 2018.

[10] K. Guo, X. Li, and L. Xie, "Ultra-wideband and odometry-based cooperative relative localization with application to multi-UAV formation control," *IEEE Trans. Cybern.*, to be published, doi: 10.1109/TCYB.2019.2905570.

[11] A. C. Woods and H. M. La, "A novel potential field controller for use on aerial robots," *IEEE Trans. Syst., Man, Cybern., Syst.*, vol. 49, no. 4, pp. 665–676, Apr. 2019.

[12] C. J. Ru, R. X. Wei, J. Dai, D. Shen, and L. P. Zhang, "Autonomous reconfiguration control method for UAV's formation based on Nash bargain," *Acta Autom. Sinica*, vol. 39, no. 8, pp. 1349–1359, 2013.

[13] X. Zhang and H. Duan, "An improved constrained differential evolution algorithm for unmanned aerial vehicle global route planning," *Appl. Soft Comput.*, vol. 26, pp. 270–284, Jan. 2015.

[14] H. Duan, Q. Luo, G. Ma, and Y. Shi, "Hybrid particle swarm optimization and genetic algorithm for multi-UAV formation reconfiguration," *IEEE Comput. Intell. Mag.*, vol. 8, no. 3, pp. 16–27, Aug. 2013.

[15] W. Zhao, R. Li, and H. Zhang, "Finite-time distributed formation tracking control of multi-UAVs with a time-varying reference trajectory," *IMA J. Math. Control Inf.*, vol. 35, no. 4, pp. 1297–1318, 2018.

[16] H.-S. Shin, A. F. Antoniadis, and A. Tsourdos, "Parametric study on formation flying effectiveness for a blended-wing UAV," *J. Intell. Robot. Syst.*, vol. 93, nos. 1–2, pp. 179–191, 2019.

[17] J. da Silva Arantes, M. da Silva Arantes, and C. F. M. Toledo, "Heuristic and genetic algorithm approaches for UAV path planning under critical situation," *Int. J. Artif. Intell. Tools*, vol. 26, no. 1, 2017, Art. no. 1760008.

[18] S. A. H. Tabatabaei, A. Yousefi-Koma, S. S. Mohtasebi, and M. Ayati, "Three dimensional fuzzy carrot-chasing path following algorithm for fixed-wing vehicles," in *Proc. IEEE RSI Int. Conf. Robot. Mechatronics*, Oct. 2016, pp. 784–788.

[19] R. A. Sarker, S. M. Elsayed, and T. Ray, "Differential evolution with dynamic parameters selection for optimization problems," *IEEE Trans. Evol. Comput.*, vol. 18, no. 5, pp. 689–707, Oct. 2014.

[20] Z. Sun, J. Wu, Y. Huang, C. Li, D. Li, and J. Yang, "Path planning for GEO-UAV Bistatic SAR using constrained adaptive multiobjective differential evolution," *IEEE Trans. Geosci. Remote Sens.*, vol. 54, no. 11, pp. 6444–6457, Nov. 2016.

[21] Y.-B. Chen, G.-C. Luo, J.-Q. Yu, X.-L. Su, and Y.-S. Mei, "UAV path planning using artificial potential field method updated by optimal control theory," *Int. J. Syst. Sci.*, vol. 47, no. 6, pp. 1407–1420, 2016.

[22] V. Roberge, M. Tarbouchi, and G. Labonté, "Fast genetic algorithm path planner for fixed-wing military UAV using GPU," *IEEE Trans. Aerosp. Electron. Syst.*, vol. 54, no. 5, pp. 2105–2117, Oct. 2018.

[23] H. Wang and Y. Li, "Hybrid teaching–learning-based PSO for trajectory optimisation," *Electron. Lett.*, vol. 53, no. 12, pp. 777–779, 2017.

[24] G. D. Góez, R. A. Velásquez, and J. S. Botero, "On-line route planning of UAV using particle swarm optimization on microcontrollers," *IEEE Latin Amer. Trans.*, vol. 14, no. 4, pp. 1705–1710, Apr. 2014.

[25] Y.-J. Gong, J.-J. Li, Y. Zhou, Y. Li, H. S.-H. Chung, Y.-H. Shi, and J. Zhang, "Genetic learning particle swarm optimization," *IEEE Trans. Cybern.*, vol. 46, no. 10, pp. 2277–2290, Oct. 2016.

[26] X.-F. Liu, Z.-H. Zhan, Y. Lin, W.-N. Chen, Y.-J. Gong, T.-L. Gu, H.-Q. Yuan, and J. Zhang, "Historical and heuristic-based adaptive differential evolution," *IEEE Trans. Syst., Man, Cybern., Syst.*, to be published.

[27] R. Miranda-Colorado and L. T. Aguilar, "Robust PID control of quadrotors with power reduction analysis," *ISA Trans.*, to be published, doi: 10.1016/j.isatra.2019.08.045.

[28] R. Miranda-Colorado, L. T. Aguilar, and J. Moreno-Valenzuela, "A model-based velocity controller for chaotization of flexible joint robot manipulators: Synthesis, analysis, and experimental evaluations," *Int. J. Adv. Robot. Syst.*, vol. 15, no. 5, pp. 1–15, 2018.

[29] R. Miranda-Colorado and L. T. Aguilar, Luis, "A family of anti-swing motion controllers for 2D-cranes with load hoisting/lowering," *Mech. Syst. Signal Process.*, vol. 133, Nov. 2019, Art. no. 106253.
[30] R. Miranda-Colorado, L. T. Aguilar, and J. E. Herrero-Brito, "Reduction of power consumption on quadrotor vehicles via trajectory design and a controller-gains tuning stage," *Aerosp. Sci. Technol.*, vol. 78, pp. 280–296, 2018.
[31] E. G. Cabral-Pacheco, S. Villarreal-Reyes, and S. Villarreal-Reyes, "Performance analysis of multi-hop broadcast protocols for distributed UAV formation control applications," *IEEE Access*, vol. 7, pp. 113548–113577, 2019.
[32] J. Zhang, J. Yan, P. Zhang, and X. Kong, "Design and information architectures for an unmanned aerial vehicle cooperative formation tracking controller," *IEEE Access*, vol. 6, pp. 45821–45833, 2018.
[33] Y. Wang, T. Sun, G. Rao, and D. Li, "Formation tracking in sparse airborne networks," *IEEE J. Sel. Areas Commun.*, vol. 36, no. 9, pp. 2000–2014, Sep. 2018.
[34] F. Liao, R. Teo, J. L. Wang, X. Dong, F. Lin, and K. Peng, "Distributed formation and reconfiguration control of VTOL UAVs," *IEEE Trans. Control Syst. Technol.*, vol. 25, no. 1, pp. 270–277, Jan. 2017.
[35] Y. Zou, Z. Zhou, Z. Meng, and X. Dong, "Distributed formation control for multiple vertical takeoff and landing UAVs with switching topologies," *IEEE/ASME Trans. Mechatronics*, vol. 23, no. 4, pp. 1750–1761, Aug. 2018.
[36] Z. Wu, J. Li, J. Zuo, and S. Li, "Path planning of UAVs based on collision probability and Kalman filter," *IEEE Access*, vol. 6, pp. 34237–34245, 2018.
[37] K. Choi, D.-H. Jang, J.-H. Lee, T.-K. Chung, H.-S. Kim, and S.-I. Kang, "Hybrid algorithm combing genetic algorithm with evolution strategy for antenna design," *IEEE Trans. Magn.*, vol. 52, no. 3, Mar. 2016, Art. no. 7209004.
[38] R.-J. Wai and A. S. Prasetia, "Adaptive neural network control and optimal path planning of UAV surveillance system with energy consumption prediction," *IEEE Access*, vol. 7, pp. 126137–126153, 2019.
[39] K. Peng, J. Du, F. Lu, Q. Sun, Y. Dong, P. Zhou, and M. Hu, "A hybrid genetic algorithm on routing and scheduling for vehicle-assisted multi-drone parcel delivery," *IEEE Access*, vol. 7, pp. 49191–49200, 2019.
[40] L. Amorosi, L. Chiaraviglio, and J. Galán-Jiménez, "Optimal energy management of UAV-based cellular networks powered by solar panels and batteries: Formulation and solutions," *IEEE Access*, vol. 7, pp. 53698–53717, 2019.
[41] Q. Fan and X. Yan, "Self-adaptive differential evolution algorithm with zoning evolution of control parameters and adaptive mutation strategies," *IEEE Trans. Cybern.*, vol. 46, no. 1, pp. 219–232, Jan. 2016.
[42] S. Hui and P. N. Suganthan, "Ensemble and arithmetic recombination-based speciation differential evolution for multimodal optimization," *IEEE Trans. Cybern.*, vol. 46, no. 1, pp. 64–74, Jan. 2016.
[43] H. Liu, H. Zhao, and W. Li, "Synthesis of sparse planar arrays using matrix mapping and differential evolution," *IEEE Antennas Wireless Propag. Lett.*, vol. 15, pp. 1905–1908, 2016.

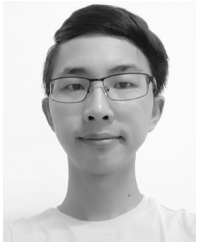

LEI BIAN is currently pursuing the master's degree with Xidian University. His current research interests include computer vision and multi-UAV control decision.

WEI SUN received the B.S. degree in measuring and control technology and the Ph.D. degree in circuit and system from Xidian University, Xi'an, China, in 2002 and 2009, respectively.

He is currently a Professor with the School of Aerospace Science and Technology, Xidian University. His current research interests include multi-UAV systems, visual information perception, pattern recognition, and embedded video systems.

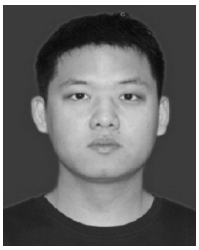

TIANYE SUN is currently pursuing the Ph.D. degree with Xidian University, Xi'an, China. His current research interests include computer vision and UAV collaborative control decision.